AERODYNAMIC INTERACTION BETWEEN A PROPELLER AND THE FUSELAGE ON A LIFT+CRUISE TYPE EVTOL AIRCRAFT

Akira Sato, Shizuoka Institute of Science and Technology, Fukuroi, Shizuoka, Japan
Jio Maruyama, Shizuoka Institute of Science and Technology, Fukuroi, Shizuoka, Japan
Koki Kitazawa, Shizuoka Institute of Science and Technology, Fukuroi, Shizuoka, Japan
Yasutada Tanabe, Shizuoka Institute of Science and Technology, Fukuroi, Shizuoka, Japan

Abstract

Numerical simulations and experimental tests have been carried out to study the performance and aerodynamic interactions between the major components on a lift + cruise type eVTOL aircraft. A two-bladed lift-rotor moving in level attitude is simulated. When the fixed-pitch propeller rotates at a constant speed, the rotor lift grows with the flying speed, while the required power is almost the same from the hover. The drag of the rotor varies significantly with the blade phase. Aerodynamic interaction between a propeller with the fuselage is also studied. It is found that when the propeller is behind the fuselage, the propulsion efficiency is improved, especially at high flight speed. However, variation in the generated thrust becomes noticeable, compared to a propeller installed in the front of the fuselage.

1. INTRODUCTION

Aerodynamic challenges in lift-and-cruise eVTOL aircraft are among the most critical barriers to their efficiency, safety, and operational viability. These issues stem from the conflicting requirements of vertical takeoff/landing (VTOL) and forward cruise phases, compounded by the complexity of transitioning between the two modes. The interaction between the fuselage and propeller(s) in eVTOL (and conventional) aircraft is a critical aerodynamic and structural consideration. This interaction affects efficiency, noise, vibration, and overall performance, particularly in lift-and-cruise eVTOL designs where propellers must operate in multiple flight phases (hover, transition, cruise).

The interaction between fuselage and propeller has been studied by many researchers so far. Among them,Troller reported the influence of fuselage on propeller design back in 1928. [1] In recent years, interests on the effect of fuselage boundary layer ingestion rise. Mikic et al compared the pusher propulsion with a tractor propeller before the fuselage for optimal efficiency. [2] Gubskiy et al carried out aerodynamic interference optimization of the fuselage-pushing propeller configuration. [3] The unsteady load caused by a proximal propeller was studied by Zamna et al. [4] A pusher propeller affected by the wake of a wide fuselage was numerically simulated and compared to the isolated propeller by Kang et al. [5]

For a typical lift + cruise type eVTOL aircraft under study by the authors as shown in Fig. 1, during hover and low-speed flight, the lift-rotors generate a high-velocity downwash during vertical takeoff/landing. This flow may strike the fuselage, wings, or other structures, causing increased download where fuselage surfaces disrupt the downwash, creating turbulent wakes and reducing net lift efficiency. Downwash can reflect off the ground or fuselage, recirculating into the propeller disk, risking vortex ring state or thrust loss. The wake from the lift-rotors may direct wash over the tail or wings, destabilizing the aircraft in hover. The authors have studied this issue through numerical simulation and experiment in hover [6]. A lift rotor in level forward flight is numerically studied in this paper.

Figure 1: Scaled-down model of a lift + cruise type eVTOL aircraft under test in SIST.

This research also focuses on the interaction between the propeller and the fuselage during transition and cruise modes. The fuselage generates a boundary layer of slower-moving air. Propeller positioned behind the fuselage (e.g., pusher configuration as shown in Fig. 1) ingests this turbulent, low-energy airflow, causing variations in the thrust and other interactions. The propeller accelerates airflow over adjacent fuselage sections. This can improve flow attachment on the fuselage but the accelerated flow may increase the skin friction which leads to a higher drag of the fuselage.

Numerical simulation and wind tunnel testing are carried out to study the aerodynamic interaction between the fuselage and the propeller to identify the change in the performance of the propeller and the fuselage. The results are compared to a propeller installed ahead of the fuselage.

Table 1: Numerical methodologies

	Background Cartesian grid	Body-fitted grid
Governing equations	Compressible Navier-Stokes equations	
Spatial discretization	Cell-vertex finite-volume method	Cell-centred finite-volume method
Numerical flux	mSLAU	
Reconstruction	FCMT interpolation method	
Viscous flux	second-order central difference scheme	
Time integration	explicit four-stage R-K method	DTS/LU-SGS
Turbulence model	Menter k-ω SST 2003 model + γ-Reθ Transition Model	

2. NUMERICAL METHODOLOGIES AND EXPERIMENTAL SET-UPS

2.1. CFD solver and numerical schemes

Numerical simulations are carried out using rFlow3D, a CFD code developed at JAXA specifically for application to rotorcraft. [7-10]. Numerical methodologies adopted for this study are listed in table 1. An all-speed numerical scheme, mSLAU [11], which stands for modified SLAU [12], is utilized, making this code also applicable to low Mach number, low Reynolds number flows associated with the small propellers.

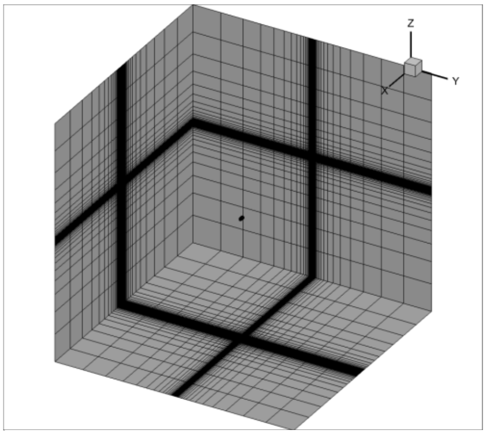

(a) Overall grid system

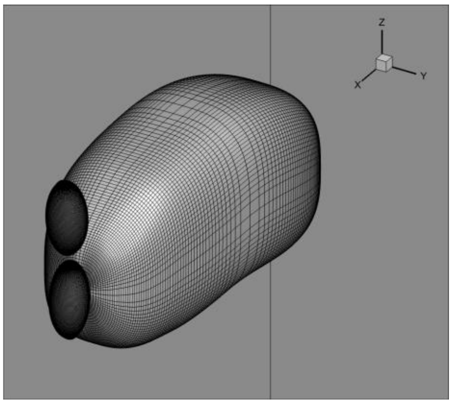

(b) Outer surfaces of fuselage and propeller

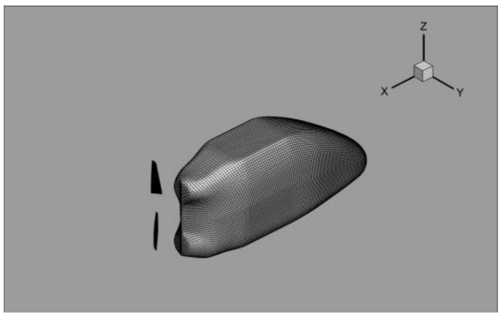

(c) Fuselage and propeller surface

Figure 2: Overlapping grid system

2.2. Overlapping grid system

Moving overlapping grid system is adopted to simulate the rotating blades. The grid system utilized for the fuselage and pusher-propeller interaction is shown in Fig. 2. Overall Cartesian background grid is built to cover a 100 times of the rotor diameter cubic space to ensure the preservation of the free-stream conditions as shown in Fig. 2 (a). Outer surfaces of the inner fuselage and blade grid are shown in Fig. 2 (b) where the inner grid area will not interfere with the physical fuselage and the rotating blades shown in Fig. 2 (c).

2.3. Experimental set-ups

Experiments are performed in a wind-tunnel as shown in Fig. 3 (a) using a half-scaled fuselage and propeller model. In Fig. 3 (b), two six-component load cells are shown, one for the fuselage and one for the motor-driven propeller individually so that the forces and moments act on the fuselage and propeller can be measured separately.

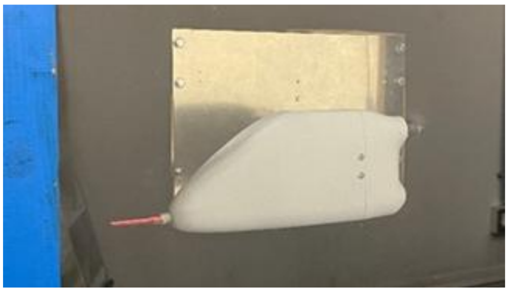

(a) Fuselage and propeller model in wind-tunnel.

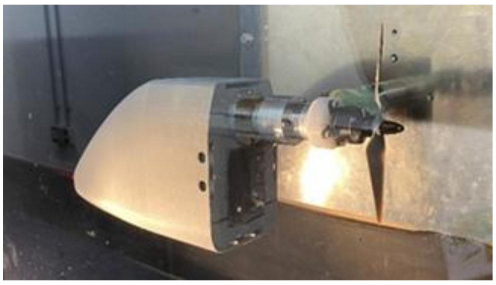

(b) Load cells inside the model.

Figure 3: Experimental apparatus for fuselage and propeller interaction study.

Nondimensionalization of the thrust, drag, torque and other forces and moments acting on the lift rotor and the propeller are based on the rotor area and the rotor/propeller tip speed.

3. RESULTS AND DISCUSSIONS

3.1. Lift-Rotor

APC 13x4E propellers are used as the lift-rotors on the aircraft. At a constant rotating speed of 7000 rpm, the flowfields change significantly with the forward flight speed as shown in Fig. 4.

The coefficients of thrust, power, and drag, and the effective lift to drag ratio, L/De, vs the advance ratio, μ, are shown in Fig. 5. It is noteworthy that the thrust (lift) grows with the advance ratio (Fig. 4 (a)) while the power is almost the same when the rotor tip-path-plane is kept level as shown in Fig. 4 (b). The drag and L/De grow almost linearly with the advance ratio as shown in Fig. 4 (c) and (d).

The coefficients of thrust, power, and drag, and the effective lift to drag ratio, L/De, vs the advance ratio, μ, are shown in Fig. 5. It is noteworthy that the thrust (lift) grows with the advance ratio (Fig. 4 (a)) while the power is almost the same when the rotor tip-path-

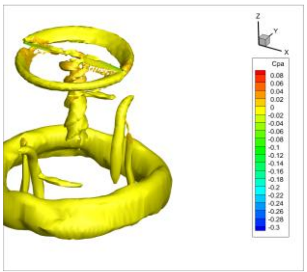

V=0m/s

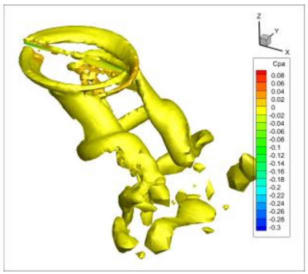

V=5m/s

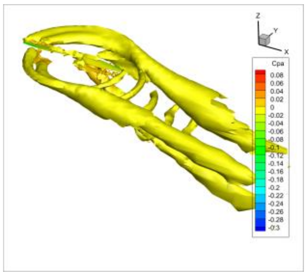

V=10m/s

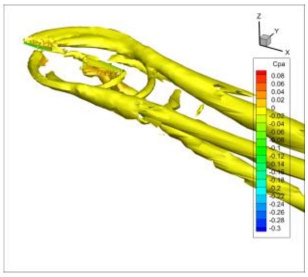

V=15m/s

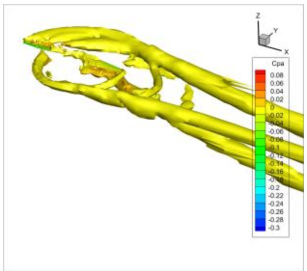

V=20m/s

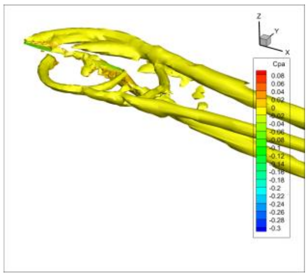

V=25m/s

Figure 4: Lift-rotor flow field change with forward flight speed.

plane is kept level as shown in Fig. 4 (b). The drag and L/De grow almost linearly with the advance ratio as shown in Fig. 4 (c) and (d).

The lift, drag and torque of this two-bladed lift-rotor are periodically oscillating 2/rev with the advance ratio as shown in Fig. 6. The initial pulsive fluctuations are caused by the abrupt rotation start in the numerical simulations and they become quasi-steady after 2~4 revolutions. Especially, the drag coefficient, CX, is typically oscillating largely, and is nearly zero or even minus at some advance ratios when the blades are aligning with the flight direction (0 or 180 blade azimuth phase angles) and rise to about 10% of the thrust when the blades are at the cross phase angles (90 or 270 azimuth angles). Along with the oscillation of the lift, this may become a source of vibrations on the aircraft. It must be noted that for this kind of lift + cruise eVTOLs, the two-bladed lift rotors must be stopped and kept in the alignment with the flight direction to reduce the drag, and the effect is very significant, which can be verified from present results.

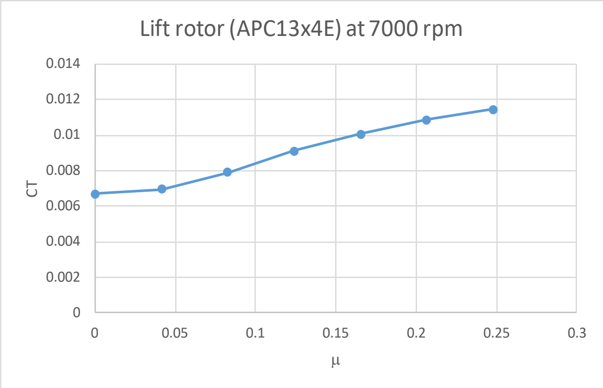

(a) Thrust coefficient

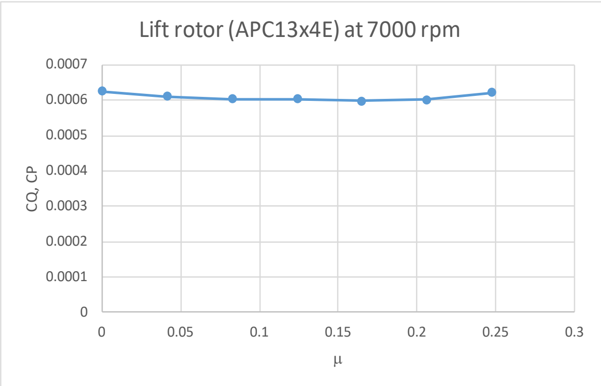

(b) Power coefficient

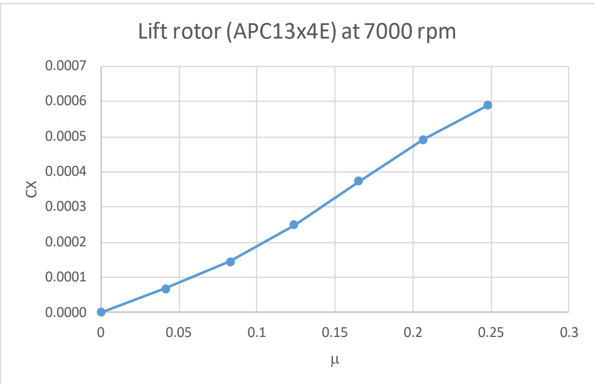

(c) Drag coefficient

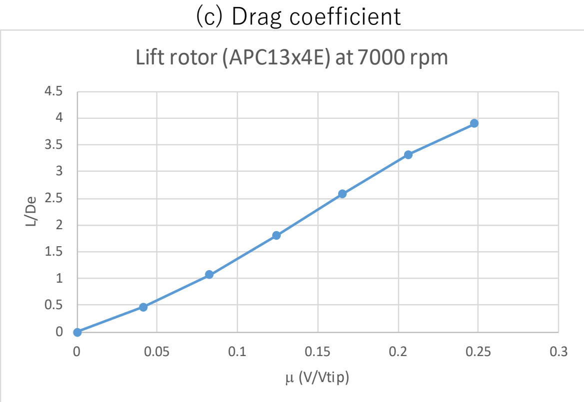

(d) Effective lift-drag ratio

Figure 5: Lift-rotor performance change with advance ratio.

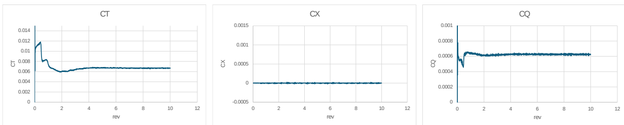

(a) μ=0 (hover)

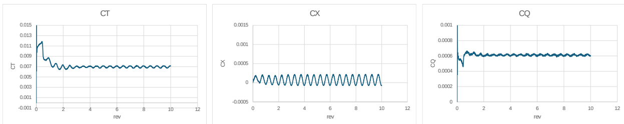

(b) μ=0.041

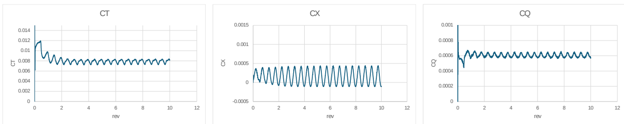

(c) μ=0.083

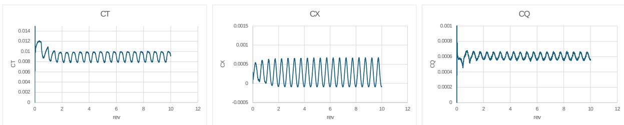

(d) μ=0.124

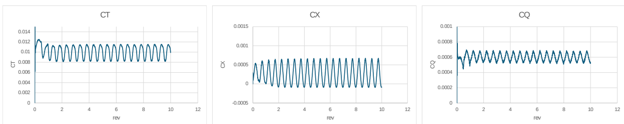

(e) μ=0.165

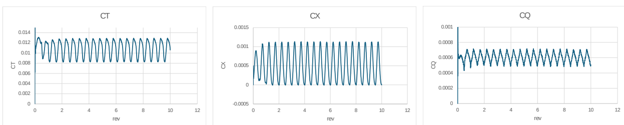

(f) μ=0.207

Figure 6: Time histories of lift, drag and torque coefficients.

3.2. Fuselage with a Pusher Propeller

The fuselage with a pusher propeller (APC 6x4E, half size for the APC 12x8E used on the aircraft) is simulated as shown in Fig. 7. The rotating speed is 14,000 rpm to keep the blade tip speed the same in the computations. The drag acting on the fuselage with a pusher propeller is compared to the isolated fuselage drag as shown in Fig. 8. It is noticed that the accelerated inflow to the fuselage caused by the propeller is especially dominant at low-speed flight.

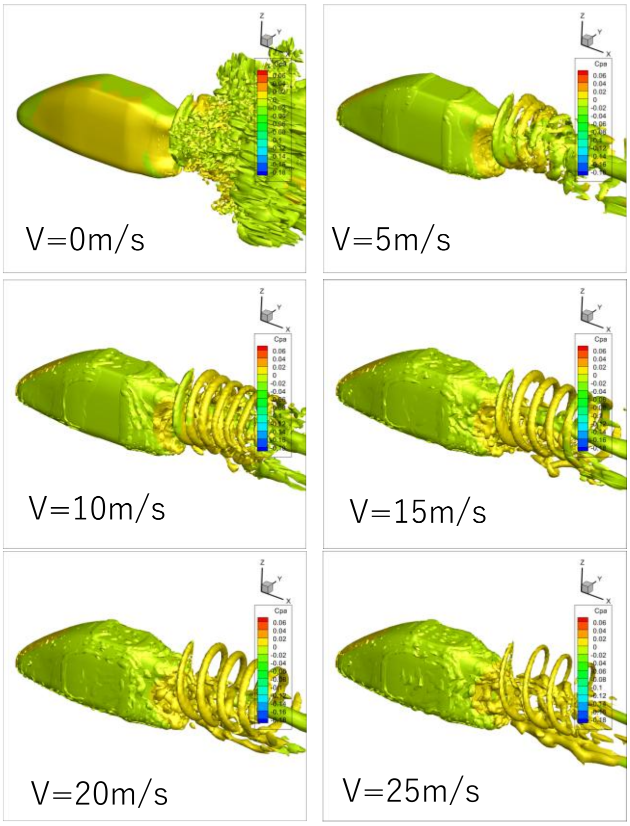

Figure 7: Flowfields of the fuselage with a pusher propeller.

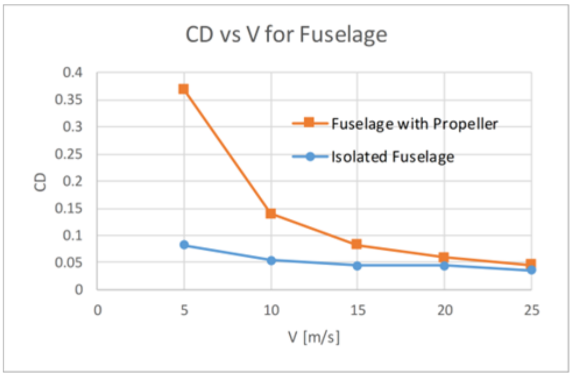

Figure 8: Drag coefficient change due to a pusher propeller.

The overall thrust estimated from the isolated propeller and fuselage results is shown in Fig. 9. No overall thrust can be generated at 25 m/s at present propeller rotating speed. The estimated overall propulsion efficiency is shown in Fig. 10. Maximum overall efficiency is at 15 m/s, compared to 20 m/s for the isolated propeller.

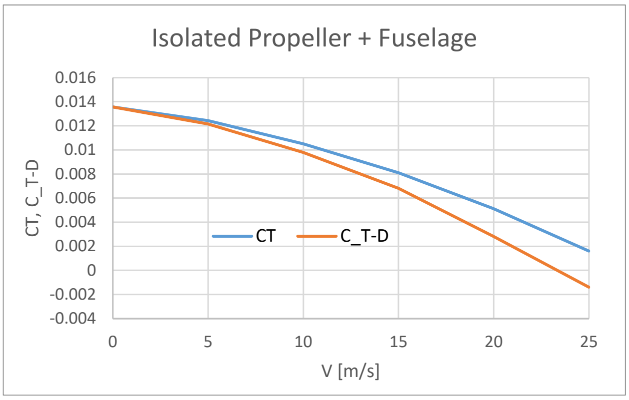

Figure 9: Overall thrust estimated from isolated propeller and fuselage data.

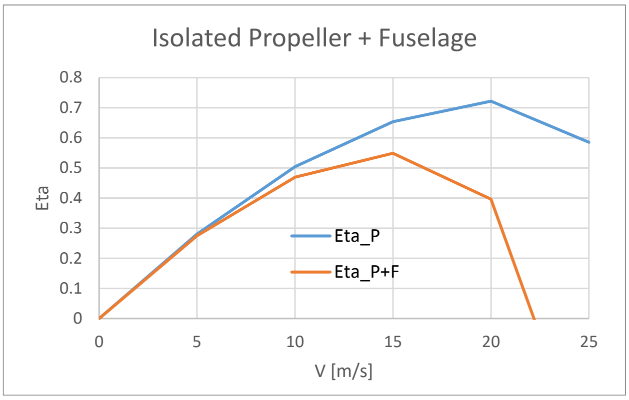

Figure 10: Overall propulsion efficiency estimated from isolated propeller and fuselage data.

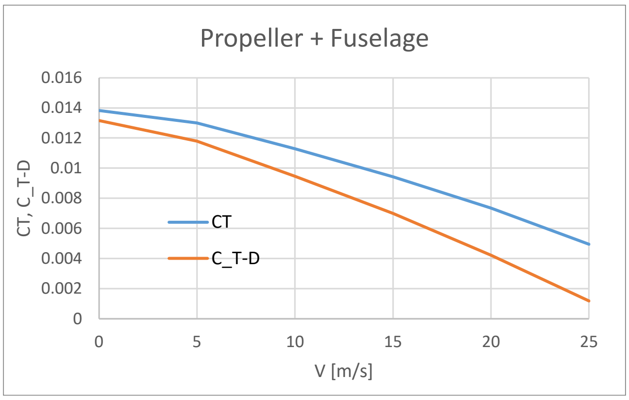

Figure 11: Thrust coefficients with fuselage and propeller interaction.

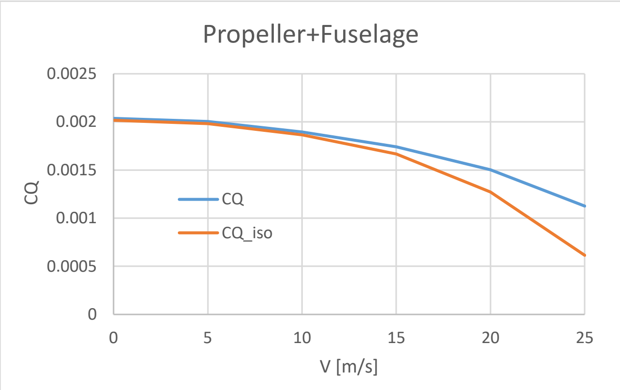

Figure 12: Torque coefficients with fuselage and propeller interaction compared to the isolated.

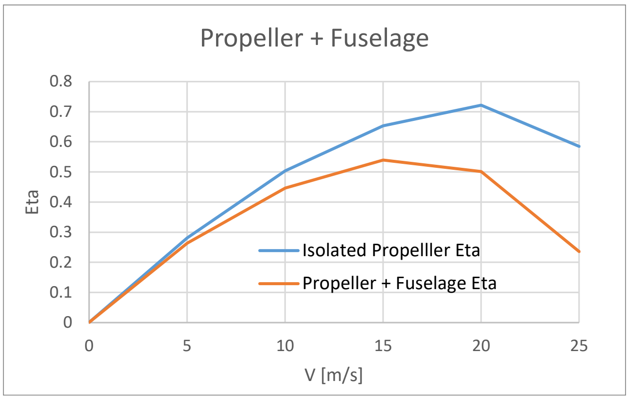

Figure 13: Propulsion efficiency with fuselage and propeller interaction.

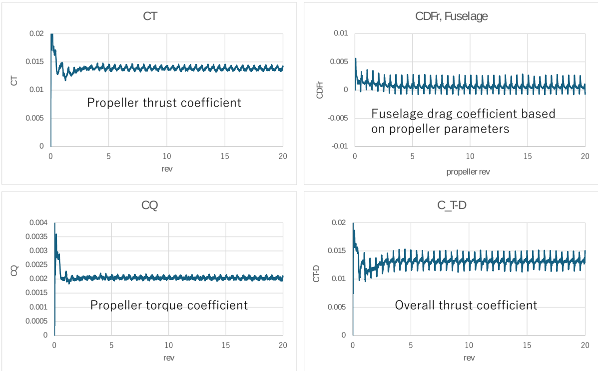

(a) 0 m/s

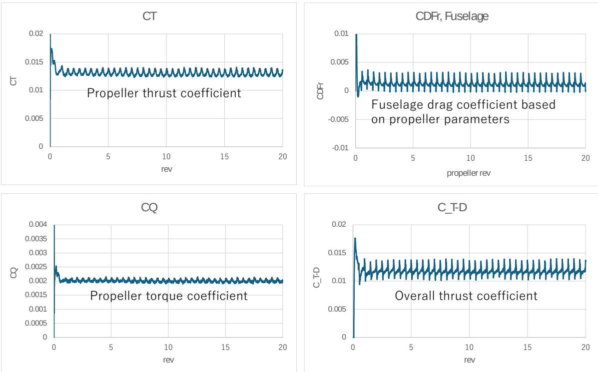

(b) 5 m/s

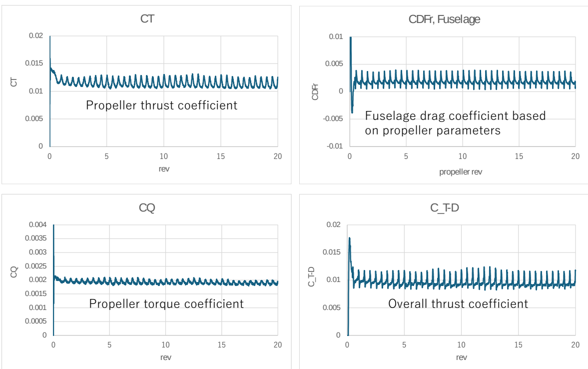

(c) 10 m/s

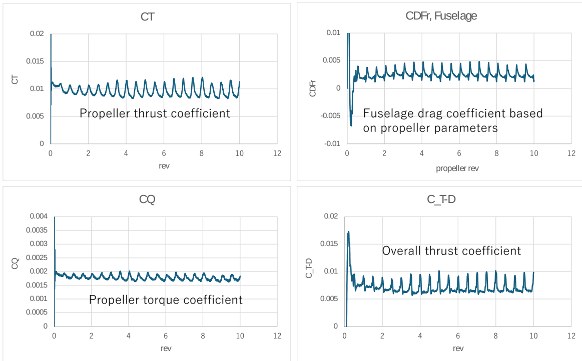

(d) 15 m/s

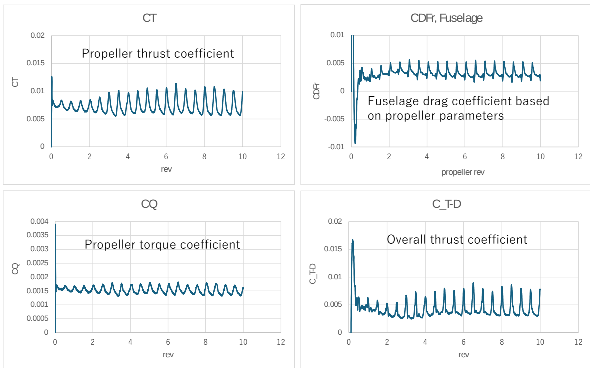

(e) 20 m/s

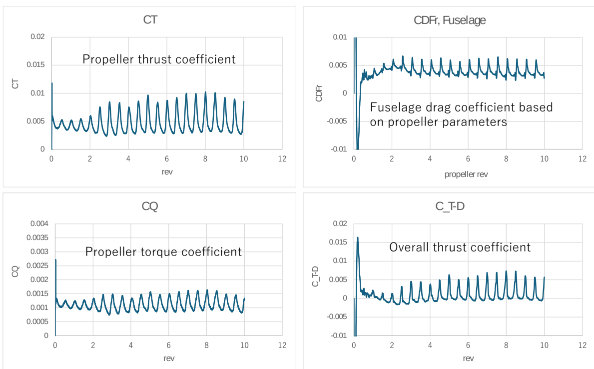

(f) 25 m/s

Figure 14: Time histories of propeller thrust, fuselage drag, torque and overall thrust coefficients for the fuselage with a pusher propeller.

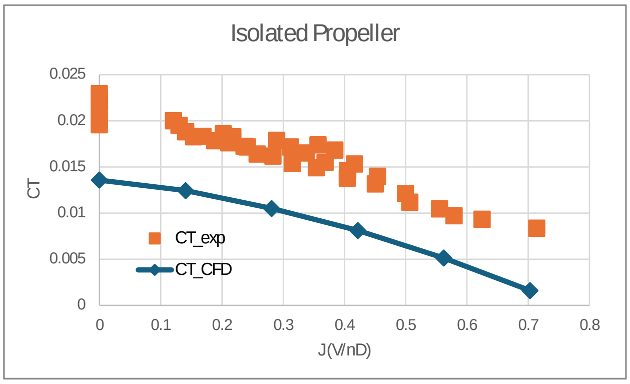

(a) Thrust coefficients comparison

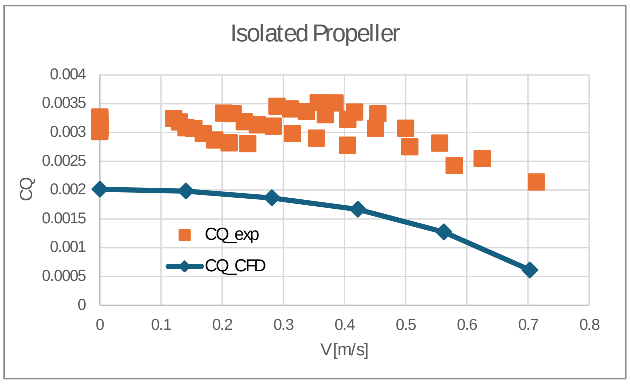

(b) Torque coefficients comparison

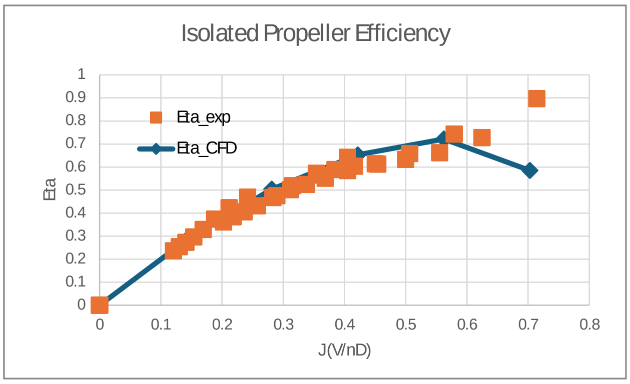

(c) Propeller efficiency comparison

Figure 15: Propeller performance measurement vs CFD analysis results.

With the interaction between the propeller and the fuselage, the thrust generated by the propeller is higher than the isolated propeller as shown in Fig. 11. The resultant overall thrust is still positive at 25 m/s. The torque coefficient is higher than the isolated propeller at high speed as shown in Fig. 12. It can be seen from Fig. 13 that the overall propulsion efficiency taking account in the interaction is higher than the values estimated from the isolated propeller and fuselage.

The time histories of the propeller thrust, fuselage drag, torque and overall thrust coefficients are shown in Fig. 14. Because the influence of the wake from the fuselage, the thrust is pulsive and becomes higher when speed increases. The fuselage drag is also pulsive (2/rev), combined with the thrust, the resultant overall thrust is also pulsive, which may incur vibrations to the aircraft.

Measurement of the isolated propeller thrust and torque was performed in a wind tunnel at various air speed and rotating speed. The results are plotted against the propeller advance ratio, J (=V/nD), as shown in Fig. 15. Both the thrust and torque are remarkably larger than the calculations. The CFD model is constructed based on the manufacturer's disclosed design data. The real shape may have certain differences. Another reason is doubt of deformation of the blade during test, because the plastic blade is very thin and soft for this small propeller. However, the propeller efficiencies shown in Fig. 15 (c) have excellent agreement between the measurement and CFD simulations.

3.3. Fuselage with a Tractor Propeller

The fuselage with a tractor propeller (APC 6x4E, half size for the APC 12x8E used on the aircraft) is also simulated for comparison as shown in Fig. 16. The rotating speed of the propeller is the same at 14.000 rpm. The wake from the propeller at 0 m/s seems largely affected by the rear fuselage.

Time histories of the propeller thrust, fuselage drag, torque and resultant overall propulsive force coefficients for this tractor propeller case are shown in Fig. 17. The time histories are noticeably smooth and no pulsive changes are observed.

The fuselage drags for the isolated, with pusher and tractor propellers are compared in Fig. 18. It is interesting to note that the tractor case is lower than the pusher case. Because of the propeller is install on the upper side of the fuselage, the wake from the tractor propeller only affects the surface of the fuselage partly.

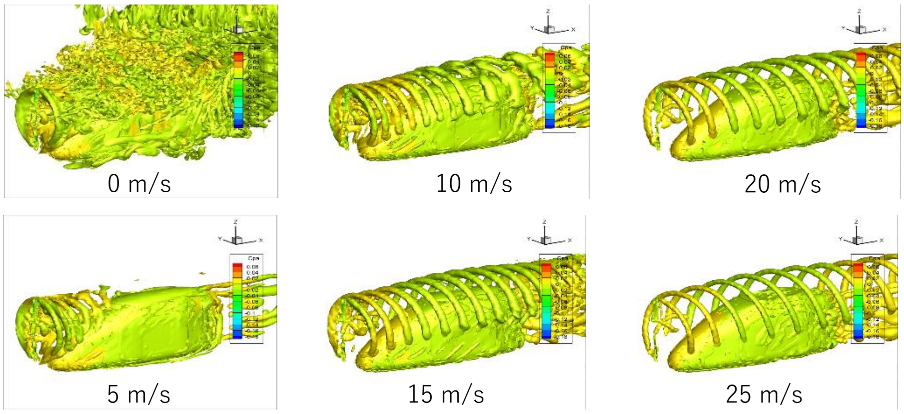

Figure 16: Flowfields of tractor propeller with the fuselage

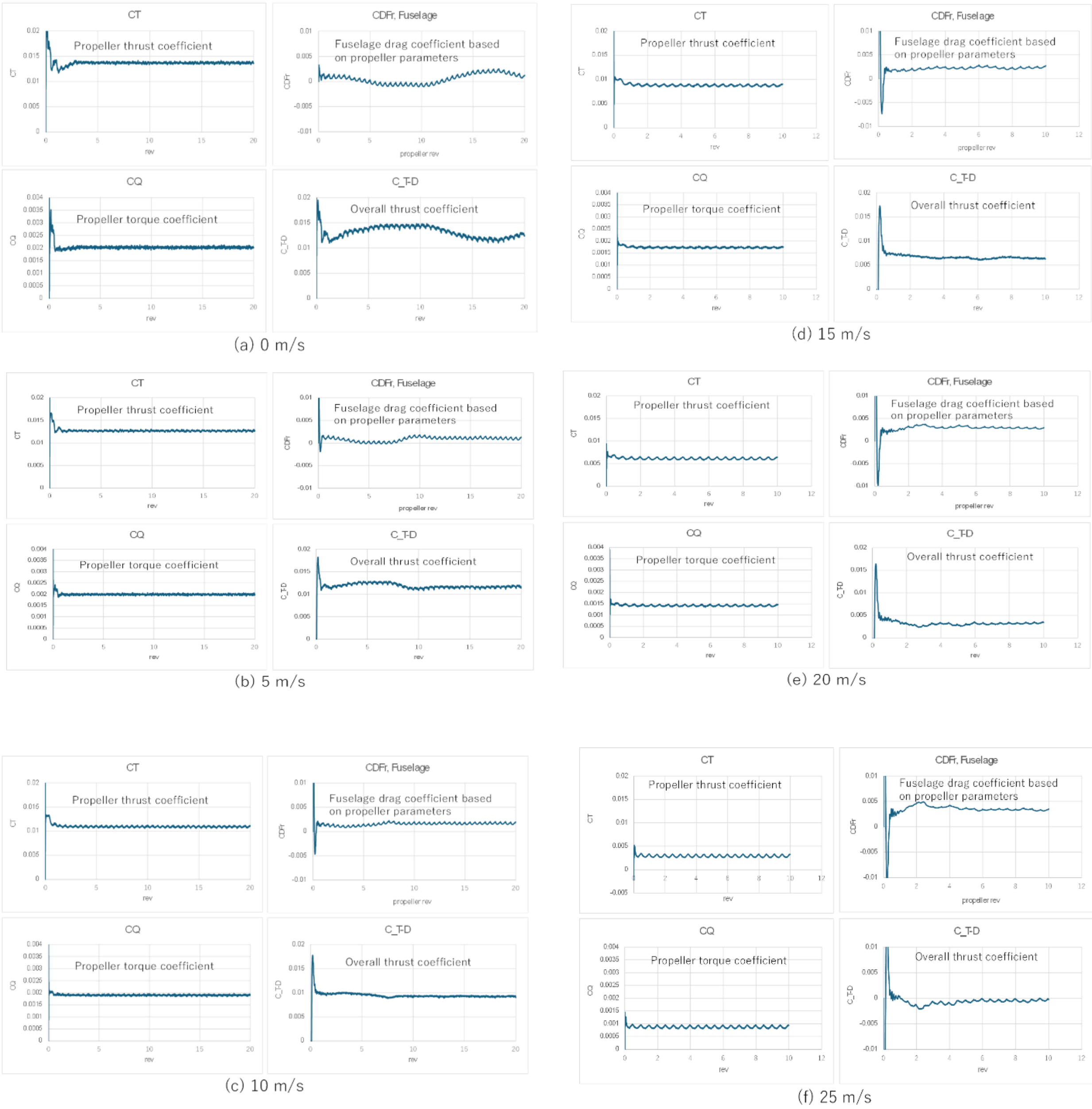

Figure 17: Time histories of thrust, fuselage drag, torque and overall thrust coefficients for tractor propeller with the fuselage

The thrust by the pusher propeller is larger than the tractor one as shown in Fig. 19. The inflow to the pusher propeller is deaccelerated by the fuselage, so the propeller can work in a relatively larger angle of attack which leads to a larger thrust generation. The resultant overall thrust is larger for the pusher propeller as shown in Fig. 20.

Torque coefficients for the two cases are compared in Fig. 21. Pusher propeller consumes more power at higher flight speed.

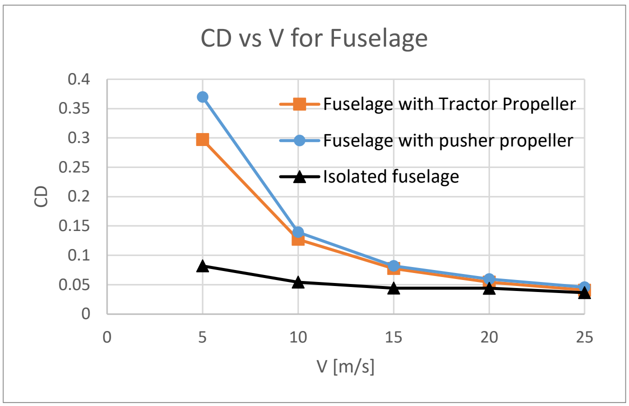

Figure 18: Drag coefficient of fuselage comparison

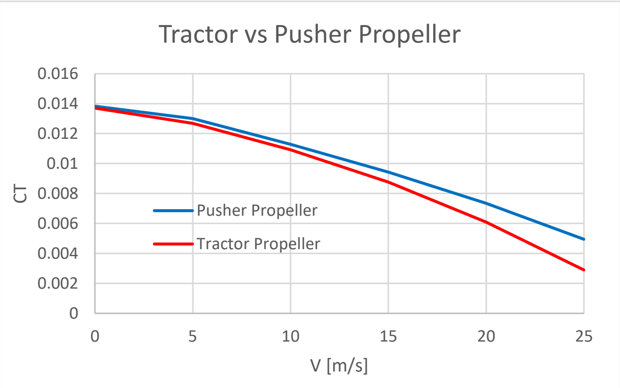

Figure 19: Propeller thrust comparison

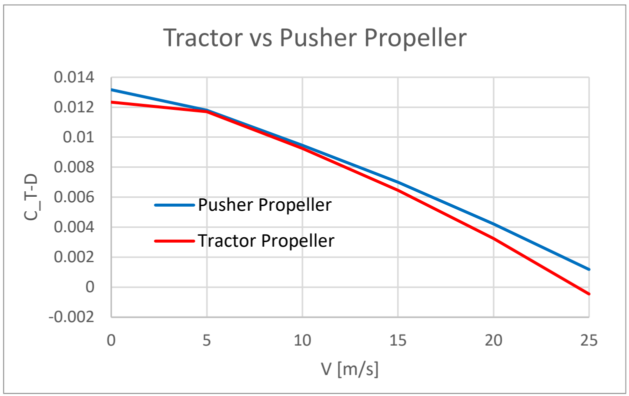

Figure 20: Overall thrust coefficients comparison

The efficiencies of the propellers themselves are compared in Fig. 22. Both are higher than the isolated propeller from the interaction with the fuselage. Efficiency of the pusher propeller increases significantly at high speed.

The overall efficiencies of the propulsion system together with the fuselage are shown in Fig. 23. Pusher propeller is advantageous in the efficiency, a factor to trade-off for the designer considering the vibratory thrust time histories.

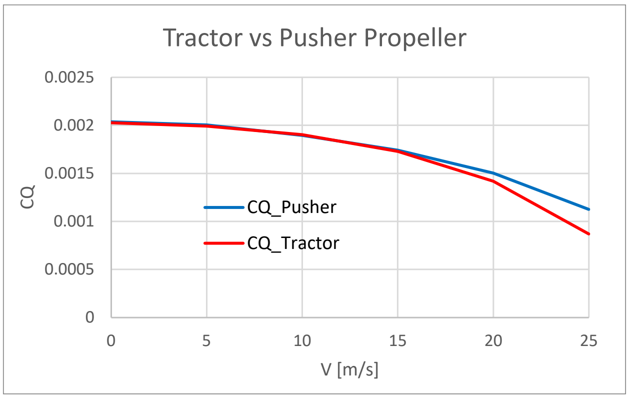

Figure 21: Torque coefficients comparison

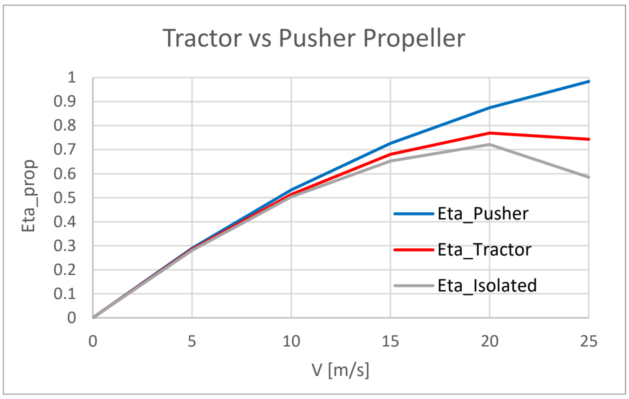

Figure 22: Propeller efficiency comparison

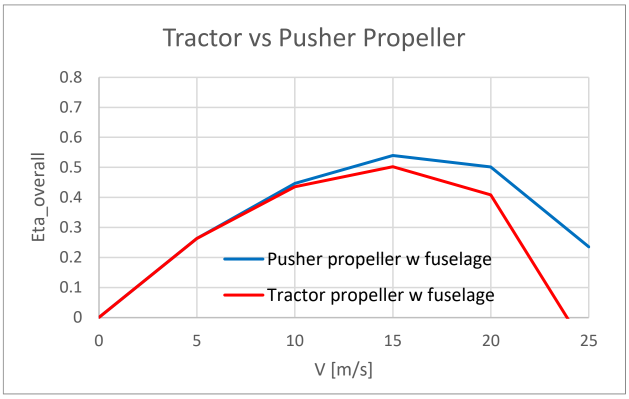

Figure 23: Overall propulsion efficiency comparison

4. CONCLUSIONS

1) A two-bladed lift-rotor moving in level attitude is simulated. When the fixed-pitch propeller rotates at a constant speed, the lift generated by the rotor grows with the flying speed, while the required power does not change from the hover. The drag of the rotor varies significantly with the blade phase angle.
2) A pusher propeller generates higher overall efficiency but the thrust is vibratory.
3) A tractor propeller can keep the efficiency similar to the isolated propeller. The thrust is relatively smooth.

Further studies with regard to the aerodynamic interactions between the lift rotors and the wing, together with the propeller and fuselage will be carried out to clarify the complex aerodynamic challenges associated with the lift + cruise eVTOL aircraft.

ACKNOWLEDGMENTS

This paper is based on results obtained from a project, JPNP23027, commissioned by the New Energy and Industrial Technology Development Organization (NEDO) in Japan.

REFERENCES

1. Troller, T., “Influence of Fuselage on Propeller Design,” NACA TM-492, 1928.

2. Mikic, G.V., Stoll, A.M., Bevirt J.B, Grah R. and Moore, M.D, “Fuselage Boundary Layer Ingestion Propulsion Applied to a Thin Haul Commuter Aircraft for Optimal Efficiency,” AIAA 2016-3764. AIAA Aviation Forum, 10 June, 2016.

3. Gubskiy, V.V, Pavlenko, O.V. and Petrov, A.V., “Aerodynamic Interference Optimization of the Fuselage-Pushing Propeller Configuration,” 2020 11th International Conference on Mechanical and Aerospace Engineering, 14-17 July 2020.

4. Zaman, I., Meloni, S, Falsi, M., Zang B. and Azarpevvand, M., “On the Unsteady Fuselage Loading Induced by a Proximal Propeller,” AIAA 2024-3380.

5. Kang, J.W., Jang J.S., You Y.H., Hyun Y.O. and Lee, J.H., “Numerical Analysis of the Effect of Fuselage of Fan-in-Body Aircraft on the Pusher Propeller.” Journal of Aerospace System Engineering 15, no. 2 (April 30, 2021): pp. 26–35.

6. Sato, A., Tanabe, Y. and Ikemoto, T., " Aerodynamic Interference Between the Lift Rotors and Main Wing on an eVTOL Aircraft, " The 10th Asian/Australian Rotorcraft Forum, Melbourne, Australia, November 7-8, 2024.

7. Tanabe, Y., Sugawara, H., "Aerodynamic Validation of rFlow3D Code with UH-60A Data Including High Advance Ratios," 41st European Rotorcraft Forum, Munich, Germany. Munich, Germany, 2015.

8. Tanabe, Y., Saito, S. and Sugawara, H., "Construction and validation of an Analysis Tool Chain for Rotorcraft Active Noise Reduction", 38th European Rotorcraft Forum, Sep. 2012.

9. Tanabe, Y., Saito, S. and Sugawara, H., "Evaluation of Rotor Noise Reduction by Active Devices Using a CFD/CSD Coupling Analysis Tool Chain", 1st Asian Australian Rotorcraft Forum and Exhibition 2012, Busan, Korea, February 12-15, 2012.

10. Tanabe, Y., Saito, S., Takayama, O., Sasaki, D. and Nakahashi, K., "A New Hybrid Method of Overlapping Structured Grids Combined with Unstructured Fuselage Grids for Rotorcraft Analysis," 36th European Rotorcraft Forum, Paris, France, September 9-11, 2010.

11. Tanabe, Y. and Saito, S., “Significance of All-Speed Scheme in Application to Rotorcraft CFD Simulations,” The 3rd International Basic Research Conference on Rotorcraft Technology, Nanjing, China. October 14-16, 2009.

12. Shima, E., and Kitamura, K., “On New Simple Low-Dissipation Scheme of AUSM-Family for All Speeds,” 47th AIAA Aerospace Sciences Meeting, Orlando, FA, January 5-8 2009, AIAA Paper 2009-136.